Continuous ground-based multiwavelength airglow measurements

R. A. Marshall,[1,2] S. Smith,[2] J. Baumgardner,[2] and S. Chakrabarti[2]

Received 1 June 2011; revised 18 July 2011; accepted 16 August 2011; published 2 November 2011.

[1] A new spectrograph instrument, called the Continuous High-resolution Instrument for Multiwavelength Echelle Spectroscopy (CHIMES), has been designed to make simultaneous and spatially overlapping ground-based measurements of the green line and red line airglow emissions (5577 Å and 6300 Å) continuously, 24 hours-a-day. The spectrograph uses a 50 mm long, 50 μm wide slit, and varies the exposure time at different times of day (daytime, twilight, and nighttime), from 2 s in daytime to 10 min at night. It utilizes an Echelle grating to achieve dispersion of 0.05 Å/pixel at 5577 Å. Daytime 6300 Å and 5577 Å airglow from this instrument are extracted by comparing the measured spectra to direct solar spectra and extracting small increases in flux in the Fraunhofer absorption lines at those wavelengths, after compensating for the Ring effect contribution. We present the first ground-based measurements of the daytime 5577 Å airglow, as well as example measurements of daytime, twilight, and nighttime airglow signatures.

Citation: Marshall, R. A., S. Smith, J. Baumgardner, and S. Chakrabarti (2011), Continuous ground-based multiwavelength airglow measurements, *J. Geophys. Res.*, *116*, A11304, doi:10.1029/2011JA016901.

1. Introduction

[2] Optical observations of the Earth's upper atmosphere in the visible part of the spectrum have been used to monitor its dynamic activity for several decades. Observations in the mid-, low-, and equatorial latitudes are used to measure thermospheric winds and temperatures [*Shepherd et al.*, 1978; *Meriwether et al.*, 1986], and these measurements are in turn used to monitor traveling ionospheric disturbances and equatorial plasma bubbles [e.g., *Valladares et al.*, 2009; *Makela et al.*, 2010]. Imaging techniques have been used to monitor gravity wave activity [e.g., *Smith et al.*, 2000]. At mid- and high latitudes, observations of the aurora are used to study the energy inputs from the solar wind and magnetosphere into the upper atmosphere. A variety of optical techniques have been developed and utilized over the years, including imaging, meridian-scanning photometry, Fabry-Perot interferometry, and spectroscopy. High-speed and stereoscopic imaging have also been utilized to establish altitudes of auroral features.

[3] The vast majority of optical observations have been made under nighttime conditions, as the large background sky signal in the daytime ($1 - 5 \times 10^6$ R/Å) makes detection of few kR airglow and auroral signatures very difficult. However, satellite measurements of the 6300 Å airglow in daytime have been made on the Atmospheric Explorer (AE) satellite [*Hays et al.*, 1978], and satellite measurements of daytime airglow in both 6300 Å and 5577 Å oxygen emissions have been made using the WINDII instrument on the UARS satellite [*Shepherd et al.*, 1993; *Shepherd*, 1996; *Shepherd et al.*, 1997]. Daytime airglow emissions of OH, O_2 and CO_2 have also been made using the SABER instrument on the TIMED satellite [e.g., *Smith et al.*, 2010], and of O_2 with the HRDI instrument on UARS [*Hays et al.*, 1992]. The 6300 Å and 5577 Å daytime airglow has also been measured by rocket-borne instruments [e.g., *Wallace and McElroy*, 1966]. In particular, *Wallace and Nidey* [1964] reported brightnesses for the 5577 Å line of ~1 kR at 150 km using a rocket-borne spectrometer.

[4] Daytime red line emissions from the ground have been measured for decades. The first measurement of the 6300 Å emission was made by *Noxon and Goody* [1962], using spectral scanning polarimetry, who estimated the brightness to be from 2 kR to 60 kR. In the following years, ground-based measurements of the red line have been made by single etalon [*Jarret and Hoey*, 1963], dual etalon [*Bens et al.*, 1965; *Cocks and Jacka*, 1979], and triple etalon [*Barmore*, 1977] Fabry-Perot interferometry. These experiments measured red line airglow in the range a few kR to tens of kR, with some controversy; while *Jarret and Hoey* [1963] found the airglow to be 30–40 kR, *Barmore* [1977] found it to never exceed 20 kR, and *Cocks and Jacka* [1979] found a peak of only 2 kR. A single-etalon Fabry-Perot with a novel mask [*Sridharan et al.*, 1998, and references therein] has also been employed from the ground, and used to correlate the initiation of equatorial spread-F with the red line airglow signature.

[5] The first detection of green line in the twilight was made by *Megill* [1960] using a birefringent photometer; the author reported slant brightnesses from 0.7 to 4.5 kR. *Frederick et al.* [1976] reported a column brightness of over 1 kR below 150 km on certain orbits of the AE satellite.

[1]STAR Laboratory, Stanford University, Stanford, California, USA.
[2]Center for Space Physics, Boston University, Boston, Massachusetts, USA.

0148-0227/11/2011JA016901

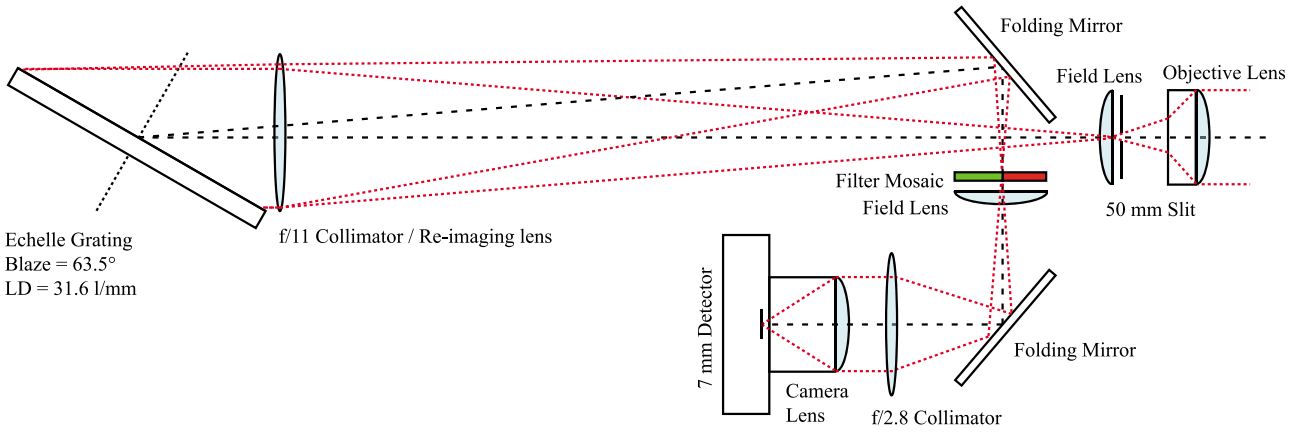

Figure 1. Layout of the Continuous High-resolution Instrument for Multiwavelength Echelle Spectroscopy (CHIMES).

Wallace and McElroy [1966] reported rocket measurements with column brightnesses of 3 kR in the green line. For a more complete history of daytime airglow measurements, including both red and green lines, we refer the reader to the review by *Chakrabarti* [1998]. A detailed description of sources of O(^{1}S) and O(^{1}D) excited states in the daytime upper atmosphere is provided by *Wallace and McElroy* [1966].

[6] In the past decade, Boston University (BU) has established ground-based measurements of daytime airglow using an instrument known as the High Resolution Imaging Spectrograph using Echelle grating (HIRISE) [*Pallamraju et al.*, 2002]. This instrument makes use of the high dispersion of Echelle gratings to measure the 6300 Å emission of O(^{1}D) at a resolution of 0.12 Å FWHM. By taking into account knowledge of the solar Fraunhofer lines and a technique to estimate the Ring effect, the HIRISE instrument is able to measure the 6300 Å emission on top of the strong day-sky background. The HIRISE instrument thus provides measurements of daytime red line using a simpler, more cost effective alternative to Fabry-Perot interferometry.

[7] A similar instrument developed at BU is the High Throughput Imaging Echelle Spectrograph (HiTIES) instrument [*Chakrabarti et al.*, 2001]. The HiTIES instrument uses the order overlap inherent to Echelle gratings to make measurements of multiple spectrally separated emissions on the same detector. In this paper, we present a new instrument, called the Continuous High-resolution Instrument for Multiwavelength Echelle Spectroscopy (CHIMES), which combines the multiwavelength nature of HiTIES with the daytime capability of HIRISE. We use this instrument to make continuous, 24-hour measurements of airglow from the ground, monitoring both the 6300 Å O(^{1}D) and 5577 Å O (^{1}S) emissions. We present the instrument design below, followed by some examples of airglow observations during daytime, twilight, and nighttime.

2. Instrument Design

[8] The instrument presented here, CHIMES, is the logical extension of the HIRISE instrument developed at Boston University [*Pallamraju et al.*, 2002]. That instrument was designed to make high-resolution daytime measurements at 6300 Å; CHIMES is designed to take advantage of order-overlap in Echelle gratings to simultaneously measure multiple wavelengths.

[9] The instrument layout is shown in Figure 1. It is based around a 100 × 200 mm, 31.6 lines/mm Echelle grating with a 63.5° blaze angle. The optical layout of CHIMES differs from HIRISE and HiTIES in that a single optical element, an1100 mm f/11 apochromat, is used for both the collimating and imaging lens, as in a classic Littrow spectrograph. An image of the slit is formed adjacent to itself, displaced in angle by ~2.6°. A folding mirror is used to wrap the image across the entrance beam, where it comes to a focus. A filter mosaic and field lens are placed at this image plane. Optics are then used to re-image the 50 mm long slit image onto the 7 mm detector using a 25 mm f/0.95 camera lens. The slit itself is ~50 μm wide. Currently, the objective is a 16 mm f/2.8 fish-eye lens (used at f/11) paired with a 50 mm focal length field lens, which yields an all-sky field-of-view; however, this front end can be easily swapped to change the field-of-view and spatial resolution.

[10] A mosaic filter is placed at the image plane as shown in Figure 1. In its current configuration, CHIMES has panels for the 6300 Å and 5577 Å lines, but the instrument design lends itself to the measurement of other lines as well. The configuration is optimized through the grating line density; grating angle with respect to the collimator; the collimator focal length; and the placement of the folding mirror. Other configurations yield different combinations of emission lines falling at different locations in the image plane. The method for determining line positions is described in detail by *Chakrabarti et al.* [2001]. The particular filters used here are 50 × 20 mm in dimension, and 40 Å FWHM in bandwidth, with ~60% and ~80% peak transmission in the red and green panels, respectively. The bandwidth of the filters is chosen to be wide enough to let in an appreciable range of wavelengths near the lines of interest, accounting for the wavelength shift with incident angle, yet narrower than the free spectral range (FSR) of the instrument; i.e., narrow enough to prevent adjacent orders from the diffraction grating interfering with the useful signal. The FSR of the instrument is 65 Å at 5577 Å; so, while 5577 Å falls at its observed position in the order 102, at the same position 5521 Å falls in order 103, and 5633 Å in order 101. Thus,

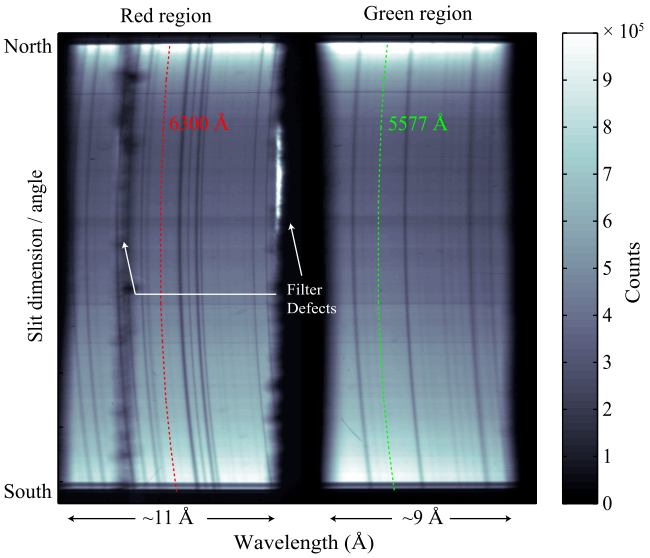

Figure 2. Example 1-minute spectra from CHIMES, taken September 20, 2010, at 1445 UT (1045 LT), in Boston, MA. This is an unprocessed image from the instrument, exhibiting the solar Fraunhofer lines in the vicinity of the 6300 Å and 5577 Å regions of the spectrum. The locations of the red and green line emission of atomic oxygen are marked by the vertical red and green dashed lines.

the 40 Å bandwidth of the filter ensures that only 5577 Å is observed at this position, and similarly for 6300 Å (where the FSR is 69 Å, and the 90th order is observed).

[11] The detector is an Atik 314L+ camera, which uses a Sony ICX-285AL CCD chip, an array of 1392 × 1040 pixels of 6.45 μm square. This small detector, while having only 65% peak QE, represents a considerable cost savings over high-end back-illuminated CCD cameras. During daytime measurements, where photon count is not an issue, this camera suits our purposes quite nicely.

[12] The instrument is set up to take 2-second exposures during the day (limited by the time to fill the CCD well), and 600-second exposures during the night, after nautical twilight. In addition, the daytime images are binned by a factor of 2 in the meridian (spatial) direction, and the nighttime images by a factor of 16. Daytime and twilight images are co-added in post-processing to yield variable time resolution images, the shortest of which are one-minute integrations. The one-minute images provide high enough SNR to reliably extract the Ring effect and 6300 Å airglow intensity during midday.

3. Data Extraction and Analysis

[13] CHIMES has been deployed and taking measurements in Boston since August 2010. An example of an unprocessed spectrum from the instrument, taken on September 20, 2010, is shown in Figure 2. The left half of the image is passed through the red filter (covering 6295–6306 Å), while the right half of the image shows the green part of the spectrum (covering 5574–5583 Å). The 6300.308 Å and 5577.345 Å line positions are marked by the dashed lines. The line curvature is a predictable effect due to oblique incidence on a grating from a long slit [*James and Sternberg*, 1969, section 5.9]. The red filter was constructed by combining two long, thin pieces of filter glass at our disposal; hence, the large defect in the middle of the spectrum is the joint between the two pieces of glass. The position of the filter has been adjusted so that this joint does not interfere with the 6300 Å line of interest, nor the set of four prominent Fraunhofer lines to its right, which are used for wavelength calibration.

3.1. Daytime Keograms

[14] During daytime, CHIMES records images with 2-second exposures. At the end of each day, images are co-added automatically to form a sequence with 1-minute time resolution. Each 1-minute "sum" image combines ~18 exposures of 2 s each, for 36 s of total exposure time per minute (the remaining 24 s are accounted for by readout in the set of exposures). In addition, at the end of each day we take a strip of data at a wavelength away from the airglow or Fraunhofer lines, and combine these to form a keogram displaying the intensity of the sky along the slit during the course of the day. Two examples of such images are shown in Figure 3, for clear and cloudy skies. The sky is considerably brighter when clouds are overhead; as such, these daily images give us a very useful summary of the sky conditions each day. Data is not recorded when the sun is directly above the slit; hence the 20-minute long blacked-out period of data in the center of each image.

3.2. Calibration

[15] CHIMES is calibrated into MR/Å (for the daytime data) through a cross-calibration with a compact spectrograph designed at BU. This compact spectrograph is exposed for ~600 seconds to a C_{14}-activated standard light source with a known brightness of ~104 R/Å at 6300 Å and ~26.6 R/Å at 5577 Å. The center of the field-of-view of this spectrograph is thus calibrated into R/Å. This same spectrograph is exposed to the daytime sky near the zenith, and compared to data taken simultaneously with CHIMES. We find that this calibration scheme yields the expected daytime zenith blue sky brightness in the range of 1–5 MR/Å, depending on solar zenith angle and sky conditions.

3.3. Daytime Data Extraction

[16] The analysis method for extracting daytime red- and green-line brightnesses is depicted in Figure 4. We co-add images to form 1-minute averages as described above; we remove hot pixels, and then this data is dark-subtracted, flat-fielded, and calibrated into MR/Å. The result is shown in Figure 4a. After separating the red and green sections of data, the first analysis step is to straighten the slit image by fitting a quadratic to a region near the emission lines of interest. The straightened data are shown in Figures 4b and 4c. The increased brightness at the horizons is due to the van Rhijn effect [e.g., *Broadfoot and Hunten*, 1966], which increases the sky brightness by about a factor of 5 on the horizons compared to the zenith.

[17] Next, focusing in on a region of data around the lines of interest, each row of data (i.e., each location on the sky) is compared to a solar spectrum taken with CHIMES. An example is shown in Figures 4d and 4e for the red 6300 Å line and Figures 4f and 4g for the green 5577 Å line. The data shown are interpolated to 0.02 Å resolution to improve the wavelength calibration of the Fraunhofer line positions;

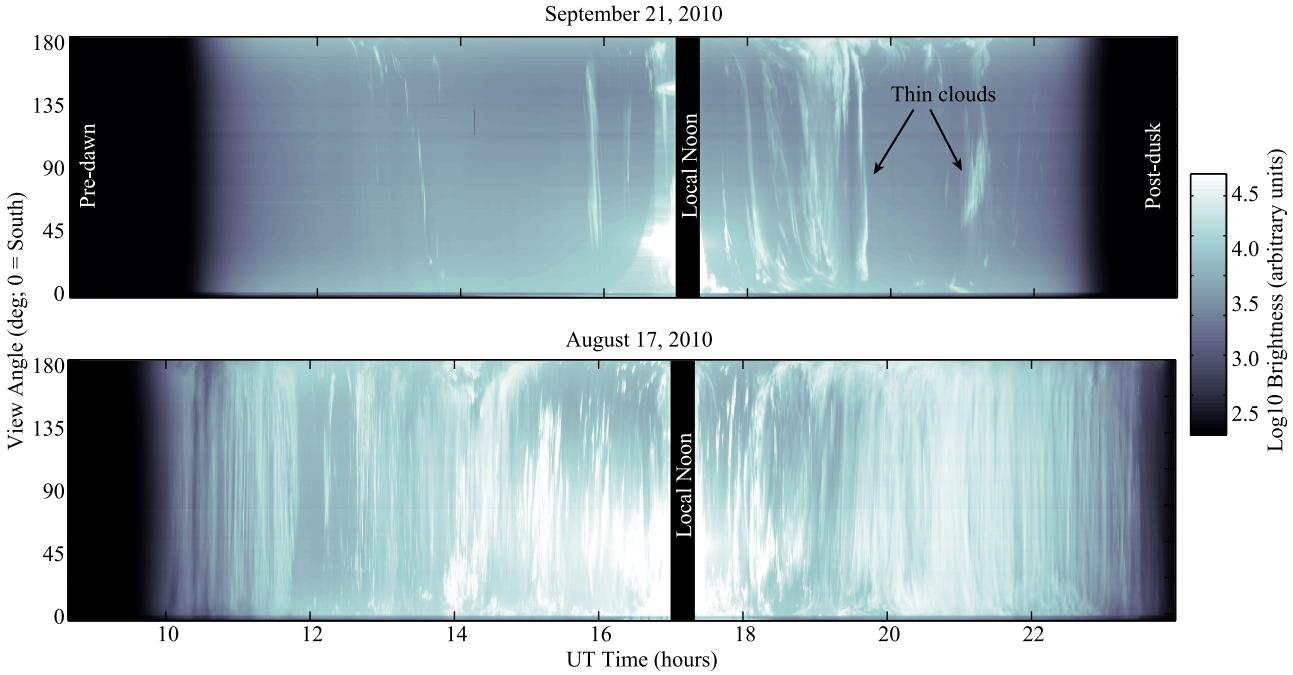

Figure 3. Example Keograms showing (top) mostly clear skies and (bottom) cloud activity. Data is not recorded when the sun is directly incident on the slit; in the cases shown here the sun crosses around 17 UT over 20 min duration. The dark regions at the left and right show data recorded before sunrise and after sunset, when the sky brightness changes by more than three orders of magnitude.

however, the original data is used to find the integrated brightness.

[18] Consider Figures 4d and 4e, for the red 6300 Å line, and specifically the two weak Fraunhofer features shown in Figure 4e. The absorption line on the left is partially filled in with respect to the solar spectrum by a combination of daytime airglow and Ring effect contribution [*Grainger and Ring*, 1962]. The Ring effect is thought to be due primarily to rotational Raman scattering from air molecules [*Pallamraju et al.*, 2002]. A thorough discussion of the Ring effect contribution to dayglow data can be found in work by *Pallamraju et al.* [2000, 2002]. For the rightmost of the two Fraunhofer features in Figure 4e, the difference between the data spectrum and a solar spectrum is the Ring effect only.In previous work, the Ring effect contribution is assumed to be very similar for Fraunhofer features of similar wavelength and line strength, and this assumption supported by observations [*Pallamraju et al.*, 2000]. Hence, in previous work, the authors integrate the difference between the data and solar spectra for each of these two features, yielding quantities *A* and *B*; respectively; the difference between these two integrations (*A* minus *B*) is the dayglow contribution in Rayleighs.

[19] This extraction method has been well established for the 6300 Å red line [e.g., *Pallamraju et al.*, 2002]. However, to our knowledge, extraction of the daytime 5577 Å green line has never before been attempted. The data and solar spectra for the green line, shown in Figures 4f and 4g, show that the emission line falls on a small Fraunhofer absorption feature, similar to the red line, but there is not a similar, clean Fraunhofer line in the vicinity. In fact, this region is complicated by the fact that our instrument function causes the line to blend somewhat with the adjacent Fraunhofer line to either side.

[20] In order to establish a method to estimate the green line Ring effect and airglow, we have derived a new general method that can be applied to any wavelength and any Fraunhofer lines. Our method relies on the result from *Pallamraju et al.* [2000] that the fractional filling-in of Fraunhofer lines due to the Ring effect is strongly correlated to the line strength and wavelength, and weakly correlated to solar zenith angle.

[21] We begin with the solar spectrum, as measured by CHIMES, and compared with the Solar Atlas flux data [*Kurucz et al.*, 1984], as shown in Figure 5. The red and green curves show the original Solar Atlas data in μW/cm^2/nm, and the black curves show the same data convolved with an instrument function with 0.1 Å FWHM. This latter spectrum agrees well with our observed solar data. Considering only the red spectrum, we integrate under the two lines of interest (between the vertical dashed lines) to determine the fractional absorption due to the Fraunhofer lines as $f_n = I_{Fn}/I_{Tn}$ for n = 1, 2. The result in percent is shown in Table 1. We can see that the effect of the instrument function is to make the lines appear slightly "filled-in" compared to the real solar spectrum. In addition, the measured solar spectrum from CHIMES is partially filled-in due to scattered light inside the instrument, and this is most prominent in the green region. Because the measured spectra include the effects of scattered light, we use these numbers (the last column in Table 1 for our airglow estimates, rather than the modeled Solar Atlas data.

[22] Next, we consider the red region data as shown in Figure 4e and integrate under the two lines, being careful to use the same wavelength limits as above for the solar

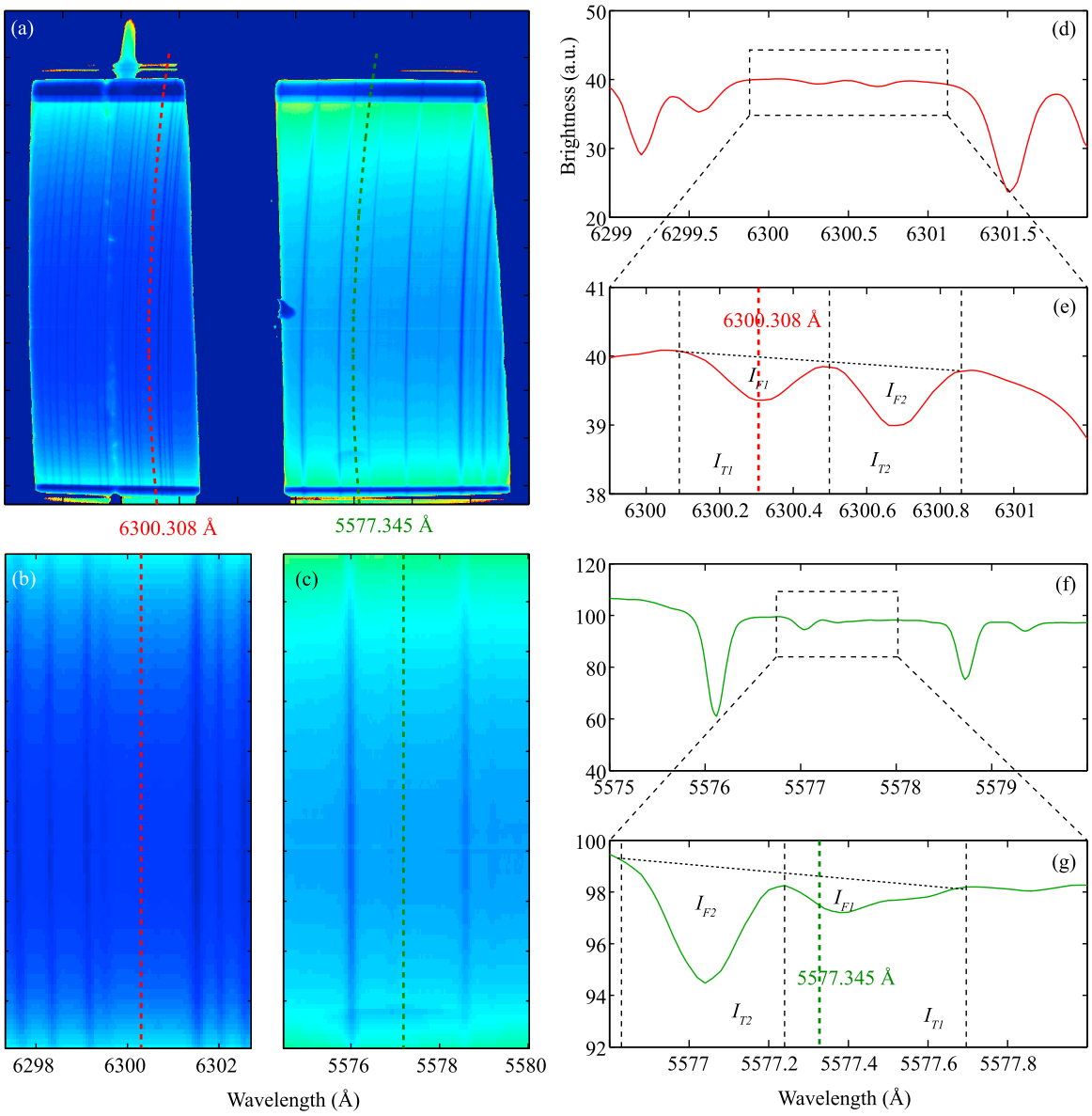

Figure 4. Dayglow data extraction. (a) A raw spectrograph image (1-minute average) after dark subtraction, flat-fielding, calibration, and hot pixel removal. (b and c) Here the lines have been straightened, the regions of interest have been extracted, and the images are calibrated in wavelength. (d and e) An average cross section in wavelength space. (f and g) The same for the green part of the spectrum. The quantities I_{F1} and I_{T1} represent the Fraunhofer absorption and the total intensity under the dashed line, respectively, in Rayleighs, for the Fraunhofer feature shown.

spectrum. Considering the line on the right, which does not have an airglow contribution, we measure the total daytime emission in this narrow band as I_{T2} in Rayleighs, and the total absorption in Rayleighs is I_{F2}, which is the area between the red curve and the dotted line. The ratio of these two $f_2 = I_{F2}/I_{T2}$ is the measured line strength, which includes Ring effect. Without the Ring effect, we would expect a measurement purely from solar Fraunhofer absorption of $I_{S2} = f_{S2} I_{T2}$, where f_{S2} is the absorption fraction in Table 1 for the 6300.7 Å line.

[23] Now, our measurement above, I_{F2}, can be written as

$$I_{F2} = I_{S2} - I_{R2} \tag{1}$$

where I_{R2} is the Ring effect contribution in Rayleighs. Now, if we were following the method of *Pallamraju et al.* [2000], we would use this same Ring effect in Rayleighs as the contribution to the line on the left. Instead, we generalize by assuming the Ring effect is proportional to the line strength; so for these two lines, $I_{R1}/I_{R2} = f_{S1}/f_{S2}$, again using the values of f from Table 1. Now, for the line on the left where the airglow contribution falls, the measured line strength is

$$I_{F1} = \overbrace{f_{S1} I_{T1}}^{\text{solar absorption}} - \overbrace{I_A}^{\text{airglow}} - \overbrace{I_{R1}}^{\text{Ring effect}} \tag{2a}$$

$$= f_{S1} I_{T1} - I_A - I_{R2} \frac{f_{S1}}{f_{S2}} \tag{2b}$$

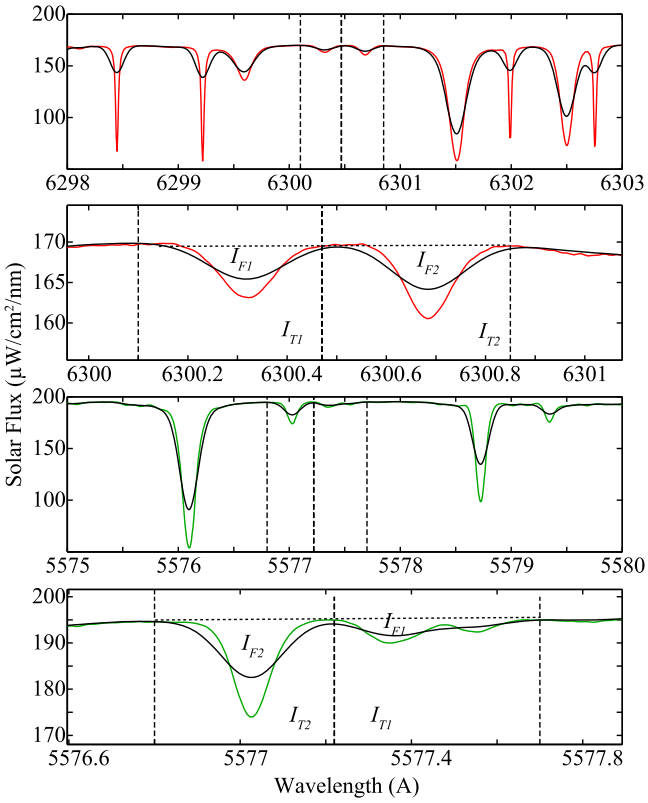

Figure 5. Solar Atlas data for the red and green regions. The red and green curves are the original data from *Kurucz et al.* [1984], and the black curves are the data convolved with an instrument function with 0.1 Å full-width at half maximum.

[24] Manipulating, we find the airglow brightness from

$$I_A = (I_{T1} - I_{T2})f_{S1} + \left(I_{F2}\frac{f_{S1}}{f_{S2}} - I_{F1}\right) \quad (3)$$

[25] Note that if the top of the spectrum were flat and the wavelength regions had equal bandwidth, so that $I_{T1} = I_{T2}$, and we assumed the line strengths to be the same, we would have $I_A = I_{F2} - I_{F1}$, which is the algorithm used by *Pallamraju et al.* [2002].

[26] This algorithm, however, can be equally applied to the green part of the spectrum shown in Figures 4f and 4g. In this case, the line strengths are most definitely not equal, and the wavelength regions do not have equal bandwidth. The bandwidth is chosen so that it spans discrete wavelengths that are unaffected by either Fraunhofer lines or airglow.

[27] A useful number to compare to is the intensity of airglow, in kR, which would be required to completely "fill" the Fraunhofer absorption lines at 6300.3 Å and 5577.3 Å. March 3, 2011 was a particularly clear day; at 1400 UT (late morning), we find a background brightness of about 2.4 MR/Å in the zenith at 6300 Å and 3 MR/Å at 5577 Å. If we scale the solar spectrum by this factor and integrate over the Fraunhofer lines, we find that the line at 6300.3 Å would be filled by airglow or aurora of ~12 kR, and the line at 5577.3 Å would be filled by ~15 kR; for the red line, this value is consistent with observations from *Pallamraju and Chakrabarti* [2005], who reported a 38 kR auroral event, which rose well above the level of the Fraunhofer absorption line. Note that this filling includes the Ring effect contribution, so that if the Ring effect in the red line is 2 kR, then 10 kR of airglow will fill the Fraunhofer line. These numbers emphasize the difficulty of trying to extract airglow intensities of a few kR or less from daytime sky spectra.

3.4. Noise Considerations

[28] Here we estimate the minimum signal that can reliably be attributed to airglow, rather than statistical fluctuations. The Sony ICX-285AL CCD sensor has a gain of about 3.75 data numbers (DN) per electron. On March 3, 2011, at 1500 UT, in the zenith, we add 2-second exposures in software to form a five-minute image, which (after dark-subtraction and flat-fielding) reports about 600,000 data numbers (DN), corresponding to 160,000 electrons per pixel. We bin in software in the meridional direction by a factor of 8, bringing the number of electrons accumulated in five minutes up to $N = 1.28 \times 10^6$ electrons per pixel. The Poisson statistical noise (shot noise) on this signal is $\sqrt{N} = 1130$ electrons, or 4240 DN. The signal of 1.28×10^6 electrons calibrates to 4.9 MR/Å at 6300.3 Å; thus, the 1130 electron noise signal calibrates to 4.3 kR/Å. At the 6300.3 Å Fraunhofer line we integrate over a bandwidth of 0.37 Å, for a total noise signal of 1.6 kR. For the green line, the total signal is $N = 3.2 \times 10^6$ electrons per pixel, which corresponds to 5.8 MR/Å brightness, and is integrated over a 0.48 Å bandwidth, for a total noise signal of 1.55 kR.

[29] Thus, ~1.6 kR corresponds to the minimum detectable signal at this time of day. At other times of day, when the sky is less bright, the noise decreases, but only by the square-root of the sky brightness. For example, on this same day at 1200 UT, the sky was ~2 MR/Å in the red region and 2.4 MR/Å in the green region, which corresponds to a noise level, and thus minimum detectable signal, of about 1 kR in both lines.

3.5. Nighttime and Twilight Data Extraction

[30] Extraction of the nighttime data is far more straightforward than the daytime data. For each 600-second exposure, we must straighten the slit image as before and calibrate into R/Å; then, we simply integrate under the lines of interest, and subtract a background intensity, defined by the baseline under the line of interest. We acknowledge that this instrument does not provide any improvements to existing measurements of nighttime airglow in the red and green lines; however, no other instrument to our knowledge measures these lines in both daytime and nighttime. The continuity

Table 1. Fraunhofer Absorption Line Strengths From Solar Atlas Data[a]

Line	*f* (Solar)	*f* (Conv.)	*f* (Data)
6300.3	1.30	0.93	0.95
6300.7	1.52	1.01	1.23
5577.0	2.74	2.65	2.37
5577.4	1.02	0.91	0.72

[a]The second column is the percent absorption from the raw data; the third column is from the convolved data; the fourth column is from measurements with CHIMES.

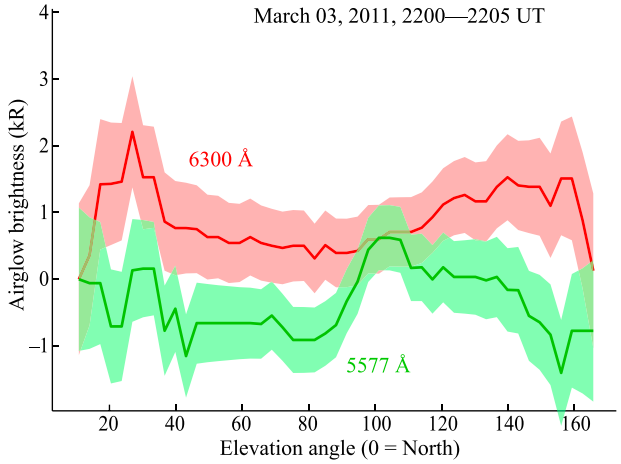

Figure 6. Measurement of daytime airglow, taken on March 03, 2011. This data results from a 5-minute integration starting at 2200 UT. The shaded regions denote the statistical shot noise level based on the sky brightness, which is dominant over other noise sources. We observe that the airglow signal in the red channel is significantly above the noise level, while the green channel is not.

provides cross-calibration between day and night emission brightnesses that can be compared to other instruments.

[31] In the twilight epoch, we observe that there is a consistent time at which Fraunhofer lines appear in the spectra; this time occurs at a solar zenith angle of 92 degrees (2 degrees below the horizon). Before this time, data is analyzed using the nighttime method, and after this time, the daytime algorithm is used. The analogous time is used to delineate night versus day at sunset.

4. Results

[32] In this section we provide first observations of airglow from CHIMES. We begin with examples of daytime data, followed by twilight and nighttime data. Our intention here is to present examples of data with some general characteristics; we will examine the implications of this data for mesospheric and thermospheric science in a later paper.

4.1. Dayglow

[33] Figure 6 shows an example of daytime airglow extracted from this data set. The figure shows a snapshot taken at 2200 UT, after averaging over 5 minutes of data. Binning leaves us with 100 data points in the meridional direction, and for plotting we apply a 8-point median filter. We observe a zenith signal of about 1 kR in the 6300 Å red line, in agreement with previous measurements. The shaded region around each curve is the noise level, as calculated in the previous section; we see that the red line brightness is strong enough above the noise to confidently constitute real airglow. In the green line, however, we measure a daytime brightness as high as 1 kR, but generally only a few hundred Rayleighs or zero Rayleighs, and this brightness does not exceed the noise level. Hence, we cannot confidently state that this measurement constitutes a real airglow signal. From the noise level, we estimate that a minimum signal of about 2 kR would be required to constitute a reliable detection of green line airglow.

[34] We next repeat this extraction process for each image taken throughout the course of the day. Figure 7 shows airglow in both emission lines for March 03, 2011. Figure 7a shows the keogram, similar to Figure 3, demonstrating that the sky above Boston was perfectly clear on this day. Figure 7b shows the airglow data for the 6300 Å line, and Figure 7c shows this same data averaged over ±15 degrees from zenith. Figures 7d and 7e show the same result for the 5577 Å line. The airglow keograms in Figures 7b and 7d are derived from 1-minute integrations of the raw data; after

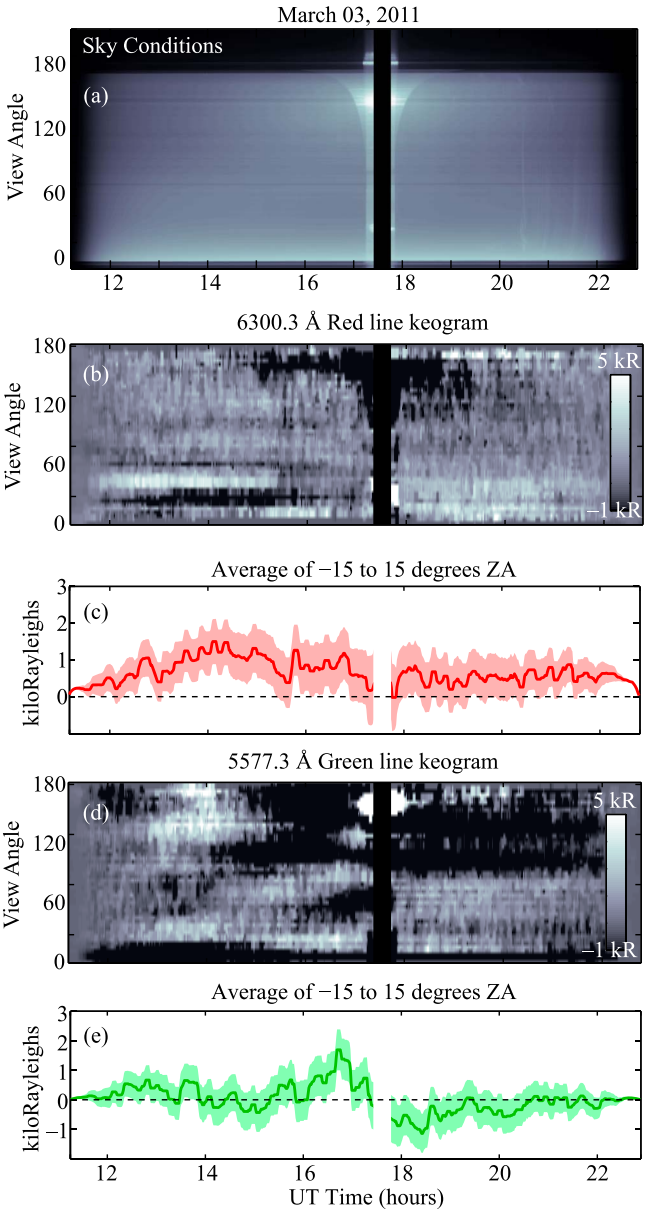

Figure 7. A full day's worth of airglow data for March 03, 2011. (a) Keogram for this day, showing clear skies for the entire day; (b) 6300 Å airglow keogram; and (c) 6300 Å airglow average over a region ±15 degrees from zenith. (d and e) The same as Figures 7b and 7c but for the 5577 Å green line.

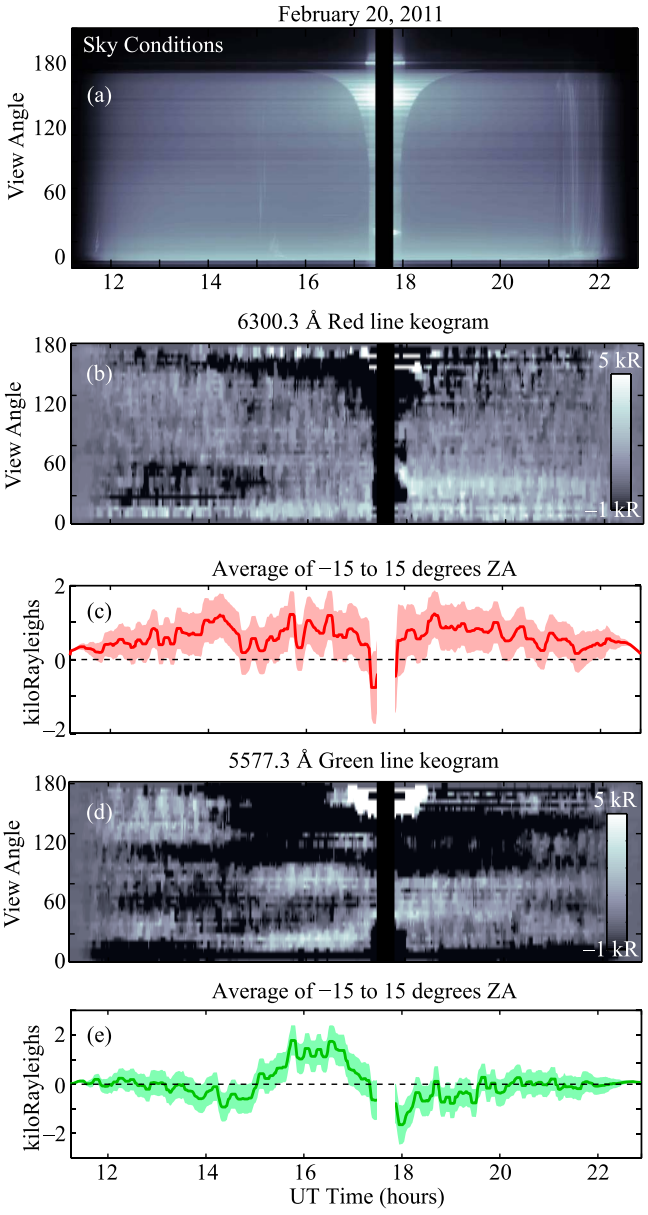

Figure 8. Same as Figure 7 but for February 20, 2011. Cloud activity on this day corrupts the airglow signal; see the text for a full description.

processing the airglow emission using the algorithm described in the previous section, the 2D result is smoothed in both the meridional and temporal dimensions with an 8-point median filter.

[35] The result shows a number of interesting features. First, in the red line emission the dayglow zenith brightness in Figure 7c shows a weak diurnal variation, similar to the results of *Pallamraju et al.* [2000], with a similar intensity, rising from the nighttime brightness of a few hundred Rayleighs up to a peak of 2 kR. In Figure 7b, we note that the red line shows very little spatial structure, except for the bright feature at 45 degrees from 12–16 UT.

[36] Figure 7d shows the green line measurement, which appears to show more spatial structure than the red line; however, we must point out that the color scale extends to −1 kR (black), in order to emphasize the 1 kR noise level. Hence, it is not certain whether the spatial structure in the green line can be attributed to airglow, or just to noise fluctuations. Figure 7e shows the green line average over ±15 degrees from zenith. Similar to Figure 6, the green line shows primarily variations around 0 kR. However, near 17 UT, just before the sun crossing the slit, the intensity reaches 2 kR, well above the noise level, which may constitute real airglow.

[37] A second example of daytime airglow is shown in Figure 8, this time for February 20, 2011, another very clear day. We observe in Figure 8b that a similar intensity and spatial structure is observed compared to March 03, except that the bright structure from 12–16 UT is absent. The same late afternoon brightening near the northern horizon is evident, though. In the profile in Figure 8c, we see a similar diurnal variation, with a peak brightness of near 2 kR.

[38] The green line also shows similar structure compared to March 03, with a bright feature near zenith from 15–17 UT. Again, it is uncertain how much of this signal can be attributed to real airglow, rather than noise fluctuations. However, this prominent feature reaches 2 kR with a <1 kR noise level with a fairly clean signal, and so it may in fact represent real green line daytime airglow.

4.2. Twilight Airglow

[39] To demonstrate the performance of CHIMES during twilight, Figure 9 shows data taken during the morning hours of March 03, 2011. On this date, the instrument transitioned from 10-minute nighttime exposures to 2-second daytime exposures at 1055 UT. For this analysis we add successive 2-second exposures to create a sequence with 5-minute resolution. Figure 9 (left) shows the extracted airglow brightness at each elevation angle. The middle and right columns show the red and green line spectra, respectively, again averaged over ±15 degrees from zenith. Time progresses downward from the top row. We can see from the first green spectra that Fraunhofer lines are already apparent, but the sky brightness is weak enough, and the airglow emission lines are strong enough to rise above the background. Over the course of the 35 minutes of data shown here, the sky brightness increases from about 10 kR/Å at 1055 UT up to nearly 700 kR/Å at 1130 UT. At 1105 UT, the sky brightness has increased to the point that the green line emission now fills in the Fraunhofer line, but does not rise above the background. The same occurs for the red line about 5 min later.

[40] The red line airglow intensity can be observed to increase from 100–500 R in the zenith at 1055 UT up to about 1 kR at 1130 UT; however, the green line maintains a level of about 100–200 R throughout the twilight epoch, while the noise level increases as the background sky brightness increases. These brightness measurements agree well with prior observations of both lines at night and of the red line airglow in the daytime [e.g., *Chamberlain*, 1995; *Pallamraju et al.*, 2000]. We also observe that the spatial structure observed is consistent over this 35 minute time period; the dip in the red line brightness near the zenith is manifested for the entire 35 minute period.

4.3. Nightglow

[41] As mentioned in the previous section, the extraction of nighttime airglow data is straightforward. We must note,

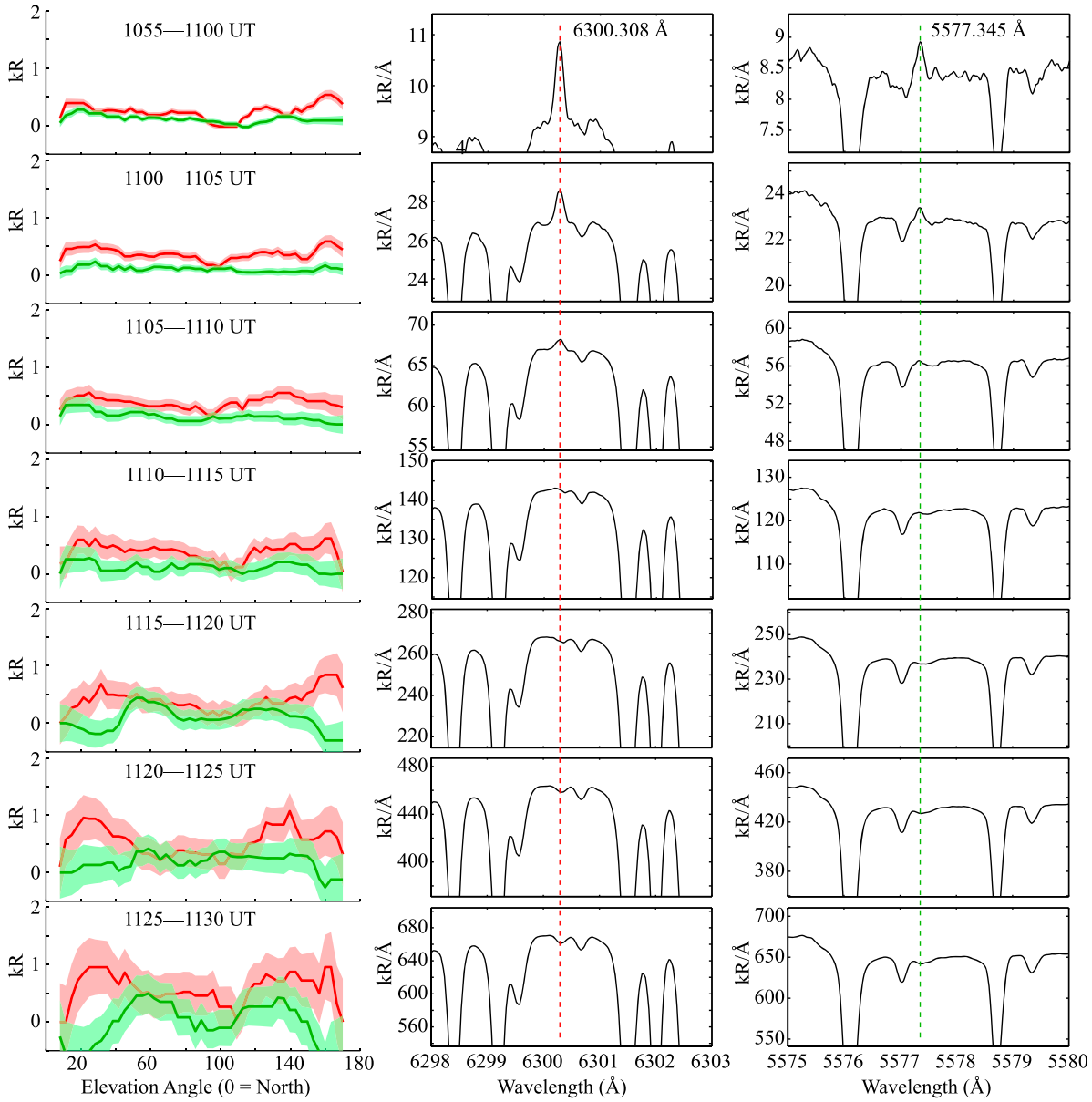

Figure 9. Airglow data passing through the twilight epoch on March 03, 2011. (left) The red and green line airglow as a function of elevation angle; (middle) a region of the red spectrum at each time; and (right) a region of the green spectrum.

however, that the instrument is not optimized for nighttime measurements. In particular, we use the same 50 μm slit for all data; however, at night this requires a long 600 second exposure in order to accumulate a clean signal. A more robust instrument might use an electronically adjustable slit width. The instrument is in fact outfitted with a "slit wheel", in essence a filter wheel with different slits in the filter positions, but this device has not been implemented. The use of this slit wheel will allow the use of a wider slit at night, and in turn shorter exposure times and higher time resolution.

[42] An example of nighttime data is shown in Figure 10 for the night of March 04, 2011; this data follows the daytime data in Figure 7 (although a one hour period from 23–24 UT on March 03 is not shown). At night, the high signal-to-noise ratio of the data allows us to easily extract spatial structures, as seen in both the red and green line keograms. The rightmost column shows "airglow" extracted from a Neon line that falls near 5579 Å. This emission comes from the city lights in Boston, and becomes prominent where there is cloud cover. This line thus acts as a reliable proxy for sky conditions at night. For comparison, we find that on cloudy nights the "airglow" in this line will reach about 1 kR, compared to the 30 R shown in Figure 10.

[43] This particular example shows weak red airglow of only a few hundred Rayleighs in the zenith, decreasing to 120 R at midnight, and increasing to 1 kR as the morning twilight appears. The green line exhibits a few hundred Rayleighs in the zenith, with some temporal variation. On

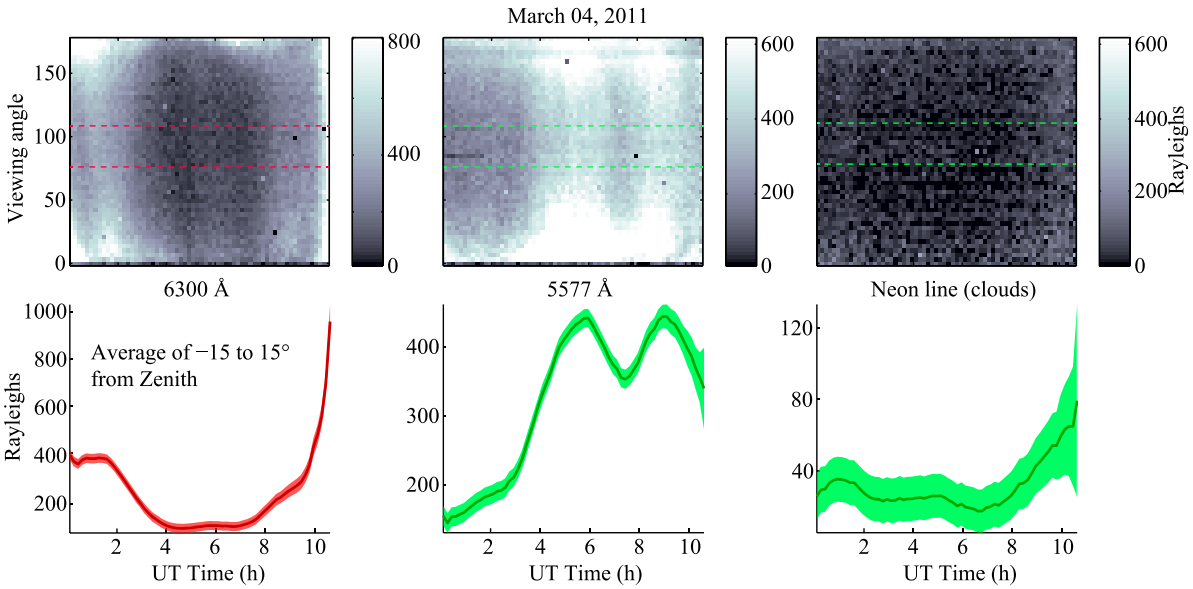

Figure 10. Example nighttime airglow data, on the night of March 04, 2011. (top) Keograms for each emission line; (bottom) an average of ±15 degrees from zenith. The right column is the "airglow" measured in a neon line that falls near 5579 Å. This line, originating from city lights in Boston, becomes prominent during cloudy nights, and is used as a proxy for the sky conditions. This particular night was very clear.

other nights, the red line airglow also reaches a few hundred Rayleighs.

5. Summary

[44] We have presented a new instrument, called CHIMES, which measures mesospheric and thermospheric airglow in multiple emission lines, continuously 24-hours a day. No prior ground- and space-based instruments are capable of measuring these emissions during an entire day. In the present incarnation of the instrument it measures the 5577 Å and 6300 Å emission lines of atomic oxygen, but the design can be easily adapted to include other emission lines. The instrument makes continuous measurements of airglow using a single slit, during daytime, twilight, and nighttime, and airglow intensities can be extracted for all time periods. As examples, we measure the red line to be a few hundred Rayleighs at night, increasing rapidly to 1 kR at sunrise, and then slowly varying diurnally between 1 and a few kR during the daytime. Similarly, the green line airglow reaches tens to a few hundred Rayleighs during the night, but does not increase as dramatically at sunrise. In the daytime, we do not measure an appreciable green line airglow above the noise level on a quiet day, except for a few cases where the signal rises to 2 kR. We estimate that a daytime auroral event with brightness of about 15 kR will completely fill in the Fraunhofer line at 5577 Å; however, a daytime airglow or aurora event of greater than 2 kR will be detectable with the CHIMES instrument.

[45] **Acknowledgments.** This work was supported by NSF grant AGS-0724440. RAM is supported by NSF CEDAR/GEM postdoctoral fellowship AGS-1027070.

[46] Robert Lysak thanks the reviewers for their assistance in evaluating this paper.

References

Barmore, F. E. (1977), High resolution observations of the 6300 Å oxygen line in the day airglow, *Planet. Space Sci.*, *25*, 185–191.

Bens, A. R., L. L. Cogger, and G. G. Shepherd (1965), Upper atmospheric temperatures from Doppler line widths—III, Observations of the O I dayglow emission at 6300 Å, *Planet. Space Sci.*, *13*, 551–563.

Broadfoot, A. L., and D. M. Hunten (1966), N_2^+ emission in the twilight, *Planet. Space Sci.*, *14*, 1303–1319.

Chakrabarti, S. (1998), Ground based spectroscopic studies of sunlit airglow and aurora, *J. Atmos. Sol. Terr. Phys.*, *60*, 1403–1423.

Chakrabarti, S., D. Pallamraju, J. Baumgardner, and J. Vaillancourt (2001), HiTIES: A high throughput imaging echelle spectrograph for ground-based visible airglow and auroral studies, *J. Geophys. Res.*, *106*, 30,337–30,348, doi:10.1029/2001JA001105.

Chamberlain, J. W. (1995), *Physics of the Aurora and Airglow*, AGU, Washington, D. C.

Cocks, T. D., and F. Jacka (1979), Daytime thermospheric temperatures, wind velocities and emission intensities derived from ground based observations of the OIλ630 nm airglow line profile, *J. Atmos. Terr. Phys.*, *41*, 409–415.

Frederick, J. E., D. W. Rusch, G. A. Victor, W. E. Sharp, P. B. Hays, and H. C. Brinton (1976), The O I (λ5577 Å) airglow: Observations and excitation mechanisms, *J. Geophys. Res.*, *81*, 3923–3930.

Grainger, J. F., and J. Ring (1962), Anomalous Fraunhofer line profiles, *Nature*, *193*, 762.

Hays, P. B., D. W. Rusch, R. G. Roble, and J. C. G. Walker (1978), The OI 6300 Å airglow, *Rev. Geophys.*, *16*, 225–232.

Hays, P. B., et al. (1992), Remote sensing of mesospheric winds with the high-resolution Doppler imager, *Planet. Space Sci.*, *40*, 1599–1606.

James, J. F., and R. S. Sternberg (1969), *The Design of Optical Spectrometers*, Chapman and Hall, London.

Jarret, A. H., and M. J. Hoey (1963), A ground-level photographic observation of the day airglow emission of atomic oxygen at 6300 Å, *Planet. Space Sci.*, *11*, 1251–1252.

Kurucz, R. L., I. Furenlid, J. Brault, and L. Testerman (1984), Solar flux atlas from 296 to 1300 nm, in *National Solar Observatory Atlas*, Natl. Sol. Obs., Sunspot, N. M.

Makela, J. J., S. L. Vadas, T. Muryanto, R. Duly, and G. Crowley (2010), Periodic spacing between consecutive equatorial plasma bubbles, *Geophys. Res. Lett.*, *37*, L14103, doi:10.1029/2010GL043968.

Megill, L. R. (1960), Photometric observations of the twilight glow [OI] 5577 and [OI] 6300, *J. Atmos. Terr. Phys.*, *17*, 276–285.

Meriwether, J. W., Jr., J. W. Moody, M. A. Biondi, and R. G. Roble (1986), Optical interferometric measurements of nighttime equatorial thermospheric winds at Arequipa, Peru, *J. Geophys. Res.*, *91*, 5557–5566.

Noxon, J., and R. Goody (1962), Observations of day airglow emissions, *J. Atmos. Sci.*, *19*, 342–343.

Pallamraju, D., and S. Chakrabarti (2005), First ground-based measurements of OI 6300 Å daytime aurora over Boston in response to the 30 October 2003 geomagnetic storm, *Geophys. Res. Lett.*, *32*, L03S10, doi:10.1029/2004GL021417.

Pallamraju, D., J. Baumgardner, and S. Chakrabarti (2000), A multiwavelength investigation of the Ring Effect in the day sky spectrum, *Geophys. Res. Lett.*, *27*, 1875–1878.

Pallamraju, D., J. Baumgardner, and S. Chakrabarti (2002), HIRISE: A ground-based high-resolution imaging spectrograph using echelle grating for measuring daytime airglow/auroral emissions, *J. Atmos. Sol. Terr. Phys.*, *64*, 1581–1587, doi:10.1016/S1364-6826(02)00095-0.

Shepherd, G. G. (1996), Application of Doppler Michelson imaging to upper atmospheric wind measurement: WINDII and beyond, *Appl. Opt.*, *35*, 2764–2773.

Shepherd, G. G., A. J. Deans, and Y. P. Neo (1978), SCIMP: A scanning interferometric multiplex photometer, *Can. J. Phys.*, *56*, 681–686.

Shepherd, G. G., et al. (1993), WINDII, the wind imaging interferometer on the upper atmospheric research satellite, *J. Geophys. Res.*, *98*, 10,725–10,750.

Shepherd, G. G., R. G. Roble, C. McLandress, and W. E. Ward (1997), WINDII observations of the 558 nm emission in the lower thermoshere: The influence of dynamics on composition, *J. Atmos. Sol. Terr. Phys.*, *59*, 655–667.

Smith, S. M., M. Mendillo, J. Baumgardner, and R. R. Clark (2000), Mesospheric gravity wave imaging at a subauroral site: First results from Millstone Hill, *J. Geophys. Res.*, *105*, 119–127.

Smith, S. M., J. Baumgardner, C. J. Mertens, J. M. Russell, M. G. Mlynczak, and M. Mendillo (2010), Mesospheric OH temperatures: Simultaneous ground-based and SABER OH measurements over Millstone Hill, *Adv. Space Res.*, *45*, 239–246.

Sridharan, R., N. K. Modi, D. Pallam Raju, R. Naranayan, T. K. Pant, A. Taori, and D. Chakrabarty (1998), A multiwavelength daytime photometer—A new tool for the investigation of atmospheric processes, *Meas. Sci. Technol.*, *9*, 585–591.

Valladares, C. E., J. Villalobos, M. A. Hei, R. Sheehan, S. Basu, E. MacKenzie, P. H. Doherty, and V. H. Rios (2009), Simultaneous observation of traveling ionospheric disturbances in the Northern and Southern hemispheres, *Ann. Geophys.*, *27*, 1501–1508.

Wallace, L., and M. B. McElroy (1966), The visual dayglow, *Planet. Space Sci.*, *14*, 677–708.

Wallace, L., and R. A. Nidey (1964), Measurement of the daytime airglow in the visual region, *J. Geophys. Res.*, *69*, 471–479, doi:10.1029/JZ069i003p00471.

J. Baumgardner, S. Chakrabarti, and S. Smith, Center for Space Physics, Boston University, 725 Commonwealth Ave., Boston, MA 02115, USA.

R. A. Marshall, STAR Laboratory, Stanford University, 350 Serra Mall, Stanford, CA 94305, USA. (ram80@stanford.edu)